Mitigating Electrolyte Flooding for Electrochemical CO$_2$ Reduction via Infiltration of Hydrophobic Particles in a Gas Diffusion Layer

Wu, Yuming; Charlesworth, Liam; Maglaya, Irving; Idros, Mohamed Nazmi; Li, Mengran; Burdyny, Thomas; Wang, Geoff; Rufford, Thomas E.

Important note
To cite this publication, please use the final published version (if applicable).
Please check the document version above.

LETTER

Mitigating Electrolyte Flooding for Electrochemical CO$_2$ Reduction via Infiltration of Hydrophobic Particles in a Gas Diffusion Layer

Yuming Wu, Liam Charlesworth, Irving Maglaya, Mohamed Nazmi Idros, Mengran Li,*
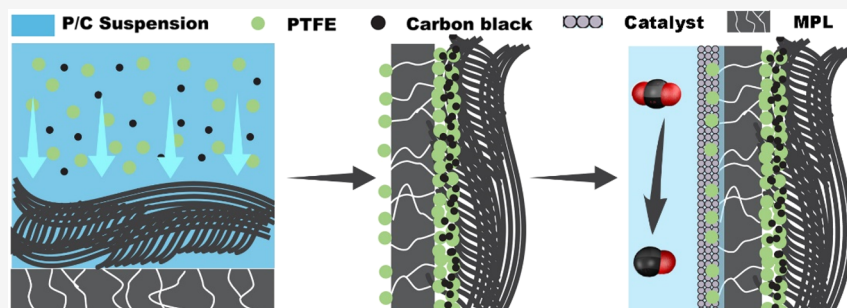Thomas Burdyny, Geoff Wang, and Thomas E. Rufford*

Read Online

ACCESS | Metrics & More | Article Recommendations | Supporting Information

ABSTRACT: Achieving operational stability at high current densities remains a challenge in CO$_2$ electrolyzers due to flooding of the gas diffusion layer (GDL) that supports the electrocatalyst. We mitigated electrode flooding at high current densities using a vacuum-assisted infiltration method to embed 200−400 nm-sized polytetrafluoro-ethylene (PTFE) particles at the interface of the microporous layer (MPL) and carbon cloth in a commercial GDL. In CO$_2$ electrolysis to CO over a silver nanoparticle catalyst on the GDL, the PTFE-embedded GDL not only just exhibited less than 10% of the electrolyte seepage rates observed in untreated GDLs at a current density of 300 mA·cm^{-2} but also expanded the electrochemical active area across the testing conditions. The PTFE-embedded GDL also maintained a Faradaic efficiency for CO$_2$ electrolysis to CO above 80% for more than 100 h at 100 mA·cm^{-2}, which was a 50-fold improvement in the stable operation time of the electrolyzer.

T he electrochemical CO$_2$ reduction reaction (CO$_2$RR) is a promising technology to reduce CO$_2$ emissions and produce valuable products,[1] such as CO, formic acid, methane, and ethylene.[2] State-of-the-art continuous CO$_2$ electrolyzers that use gas diffusion electrodes (GDEs) have been reported to achieve CO$_2$RR at industrially relevant current densities, and there are demonstrations at the pilot plant scale.[3] The GDE's porous structure facilitates CO$_2$ mass transfer from the gas phase to the liquid electrolyte and active catalyst sites at much faster rates than possible with planar electrodes.[4,5] However, managing flooding of liquid electro-lytes into the porous structure remains a critical practical challenge for GDEs with operational stability in CO$_2$ electrolyzers.

An excellent GDE for CO$_2$ electrolysis should support a high density of active catalyst sites and facilitate fast transport of gases, ions, and electrons within the electrode.[6] The most commonly used GDEs in flow-cell CO$_2$ electrolyzers have a gas diffusion layer (GDL) with carbon fiber support onto which a microporous layer (MPL) and catalyst layer (CL) are deposited.[7] The carbon fiber support (CFS) or macroporous layer is typically a hydrophobic carbon paper or carbon cloth with micron-sized pores[8] that allows fast gas transport and serves as the current collector.[9] The microporous layer is typically made with a mixture of carbon black particles and hydrophobic additives, such as polytetrafluoroethylene
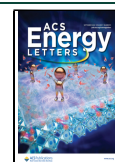
Figure 1. Infiltration of polytetrafluoroethylene (PTFE) particles in a commercial gas diffusion layer (GDL). (a) Schematic of the vacuum-assisted infiltration method. (b) Energy-dispersive X-ray spectroscopy (EDS) mapping of fluorine in the cross section of the commercial GDL (F mass% = 4.09%) and (c) in the GDL after 30% P/C infiltration (F mass% = 10.41%). (d) Scanning electron microscope (SEM) image of the surface of the microporous layer (MPL) in the GDL after 30% P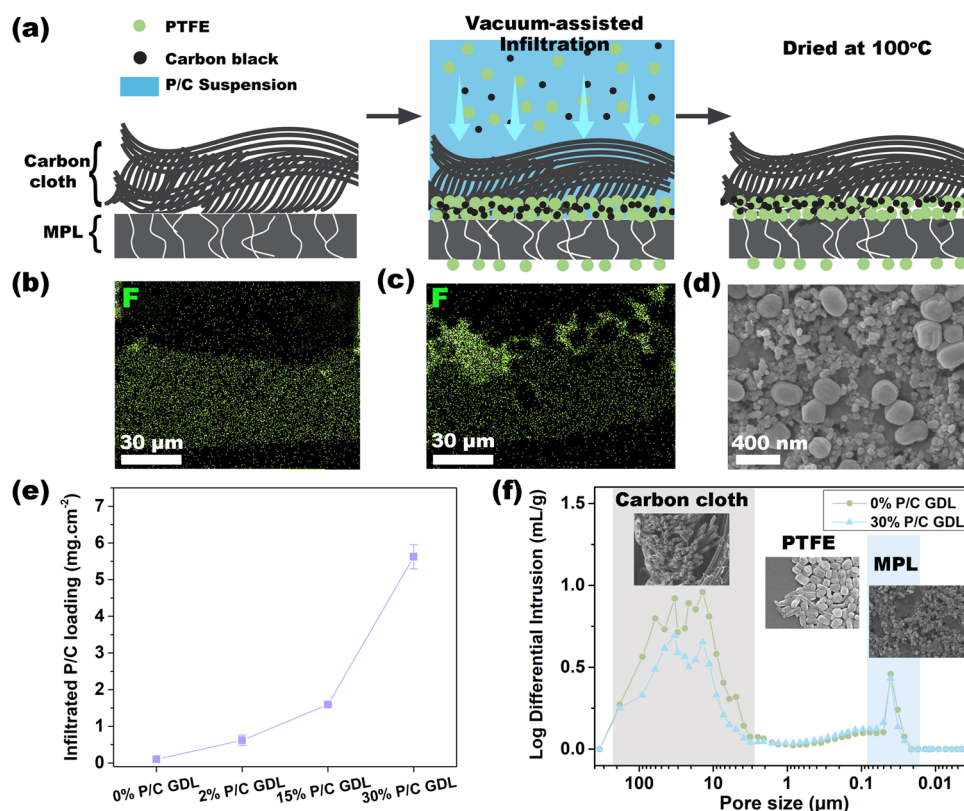/C infiltration. (e) Gravimetric loading of the PTFE and carbon black on GDLs infiltrated with suspensions of different PTFE concentrations. The error bars represent the standard deviation of three independent weightings of three samples. The X% P/C represents constant 10 mg carbon black mixed with the X% PTFE weight ratio in the 10 mL suspension for the infiltration, except 0% P/C represents 10 mL of pure water infiltrated through the GDLs. (f) Pore size distribution of the 0% P/C and 30% P/C GDLs obtained from mercury intrusion porosimetry. The particle size of PTFE in the aqueous suspension (200−400 nm) is between the pore sizes of carbon cloth and MPL.

(PTFE). The MPL plays an essential role in supporting the CL, distributing current, and preventing electrolyte flooding into the gas diffusion layer.[10,11]

Although carbon cloth GDLs are widely used in CO_2 electrolyzers, these GDLs are known to become less hydrophobic during CO_2 electrolyzer operation at highly negative potentials because of electrowetting of carbon sites under an applied electrical field,[12,13] salt precipitation,[14,15] and chemical degradation.[16] When the hydrophobicity of the GDL is reduced, electrolyte penetrates the pores of the GDL, which leads to increased distances for CO_2 diffusion and blocks CO_2 transport to CO_2RR catalyst sites. In addition, flooding can impact CO_2RR selectivity as the restriction of CO_2 transport to active sites leads to the promotion of the hydrogen evolution reaction (HER).[16−18] To date, most CO_2 electrolyzer studies used commercial GDLs that were designed and fabricated for polymer electrolyte membrane fuel cells (PEMFC) that experience very different operational conditions to CO_2RR.[10,19−22] For a PEMFC, the cathode is to convert oxygen gas to water liquid. For CO_2 electrolysis, however, the cathode is driven by the electric potential to convert CO_2 gas into either gas or liquid products, which is drastically different from the reaction scenario for PEMFC.[5,22,23] Furthermore, GDLs for PEMFCs provide the path for the water removed from the catalyst layer to gas flow channel, but electrolyte flow

is desired to be constrained in the liquid channel within the CO_2 electrolyzer.

The development of low-cost, large-scale CO_2 electrolysis technologies is more likely to be successful if CO_2 electrolyzers can take advantage of the supply chain infrastructure already developed for other applications, such as PEM fuel cells and H_2 electrolyzers. Therefore, mitigating flooding in commercial GDLs for the CO_2 electrolyzer is an urgent matter.[6,16,24] Hydrophobic treatments of microporous layers have been reported for GDLs designed for PEM fuel cells,[25,26] and there are a few recent reports on adding hydrophobic agents during fabrication of the catalyst layer on the GDL.[27,28] For example, hydrophobic additives such as fluoroalkyl silane[28] and PTFE[27,29] have been added to catalyst layers in GDEs for CO_2 electrolysis. The addition of the hydrophobic additives to the CL achieved improvements in the CO_2 electrolysis performance at short operating durations, but to date these CO_2 electrolysis improvements and hydrophobicity enhancements have not been reported to be sustained through CO_2RR stability tests at high current density.[30] Another approach that has achieved stable CO_2RR performance is replacing the carbon-based GDL with a nonconductive porous hydrophobic membrane (e.g., PTFE membranes[31,32]) coated with a conductive catalyst layer such as sputtered Cu. Electrolyzers with PTFE membranes as GDEs have demonstrated excellent
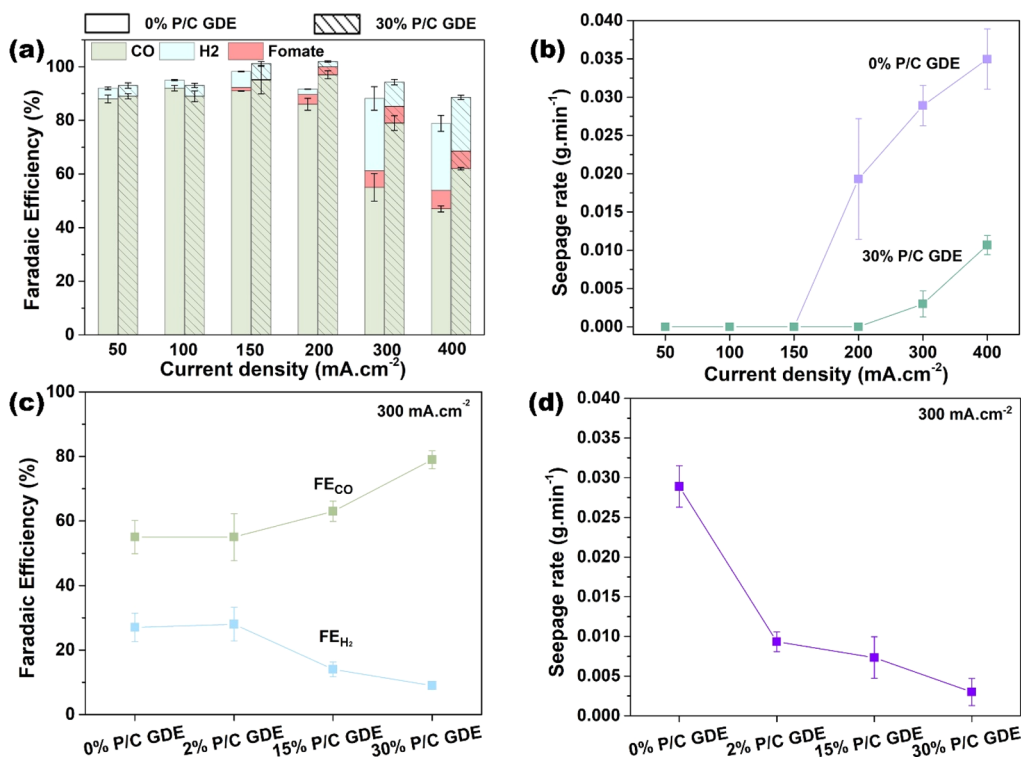
Figure 2. CO_2 reduction reaction performance of silver nanoparticle catalysts on gas diffusion electrodes (GDEs) in a gas-fed flow cell electrolyzer (Figures S10 and S11) with the catholyte of 0.1 M $NaHCO_3$ flowing at 2 mL/min and the anolyte of 1 M KOH at 10 mL/min. (a) Faradaic efficiency (FE) of the detectable CO, H_2, and formate of 0% P/C and 30% P/C GDEs. Here, GDE indicates the electrode after the Ag catalyst was sprayed onto the microporous layer of the gas diffusion layers. The X% P/C represents constant 10 mg carbon black mixed with the X% PTFE weight ratio in the 10 mL suspension for the infiltration, except 0% P/C represents 10 mL of pure water infiltrated through the GDLs. (b) Average rate of catholyte seepage through the GDEs measured during the electrolysis tests using the method in Figure S9. (c) FE for detectable CO and H_2 in CO_2 electrolysis tests with 0% P/C, 2% P/C, 15% P/C, and 30% P/C GDEs at 300 mA·cm^{-2}. (d) Average rates of catholyte seepage of the four GDEs in part (c) at a current density of 300 mA·cm^{-2}. The error bars on FEs in (a) and (c) represent the standard deviation of three measurements of electrolyzer effluent gas compositions. The error bars on seepage rates in (b) and (d) represent the standard deviation of three independent measurements on fresh GDEs for each measured current density.

CO_2RR performance at current densities of up to 1000 mA·cm^{-2},[32] but there are practical challenges to applying PTFE membranes at a large scale and low cost. Therefore, there remains a need to improve the performance of carbon-based GDLs, including the tailoring of commercial GDLs that are available at low cost for CO_2 electrolyzers.

We report a simple, vacuum-assisted infiltration method (Figure 1a) to deposit PTFE particles and carbon black preferentially at the interface between the microporous layer and the carbon cloth in a commercial GDL. The vacuum-assisted infiltration allows some PTFE particles to be transported through existing cracks in the MPL[33] and protrude into the CL to provide additional protection against electrolyte flooding through the MPL cracks. In our CO_2RR experiments with a commercial GDL and silver nanoparticle catalyst, the PTFE-embedded GDE achieved a Faradaic efficiency to CO (FE_{CO}) of nearly 80% at 300 mA·cm^{-2}. Remarkably, at 100 mA·cm^{-2} our PTFE-embedded GDE operated stably for more than 100 h with a FE_{CO} above 80%, which was more than 50 times longer than for the untreated GDE.

We introduced the PTFE particles to the commercial GDL from a suspension of PTFE and carbon black particles in water that we sucked through the GDL using a vacuum filter, as shown in Figure 1a and Figure S1. The SEM images in Figure S2 show the approximate sizes of these 9PTFE particles in the GDL were determined from the fluorine (F) signal in SEM-

EDS elemental maps of the cross section of the GDL, which was imaged by mounting the GDL in epoxy resin. First, we had to establish a benchmark for the F signal of the PTFE coating in the commercial GDL (Figure 1b). Compared to this benchmark F distribution, we can see in Figure 1c that after infiltration, there is a significantly higher concentration of F at the interface of the carbon cloth layer and the microporous layer, which shows the PTFE particles accumulate at this interface in GDL. We also observed in SEM images of the MPL face of the GDL that some PTFE particles protrude from the MPL's surface (Figure 1d). This observation suggests that some PTFE particles migrated through original cracks, up to 5 μm wide, in the MPL (Figure S4) and lodged at the underside of the MPL that pressed against the glass filter of the vacuum apparatus (illustrated in Figure S1).

We conducted a series of experiments to control the ratio of PTFE to carbon black embedded in the GDLs by modifying the composition of the suspension liquid, as shown in Figure 1e. The loading increases with the weight percentage of PTFE up to 5.6 ± mg·cm^{-2} for the 30% P/C suspension. Along with the weight percentage of PTFE, the density of the PTFE protrusions from MPL can be controlled as well (as shown in Figure S5).

The location of PTFE particles in the modified GDLs was also analyzed by characterizing the pore size distribution (PSD) of the carbon cloth and MPL layers. The PSDs
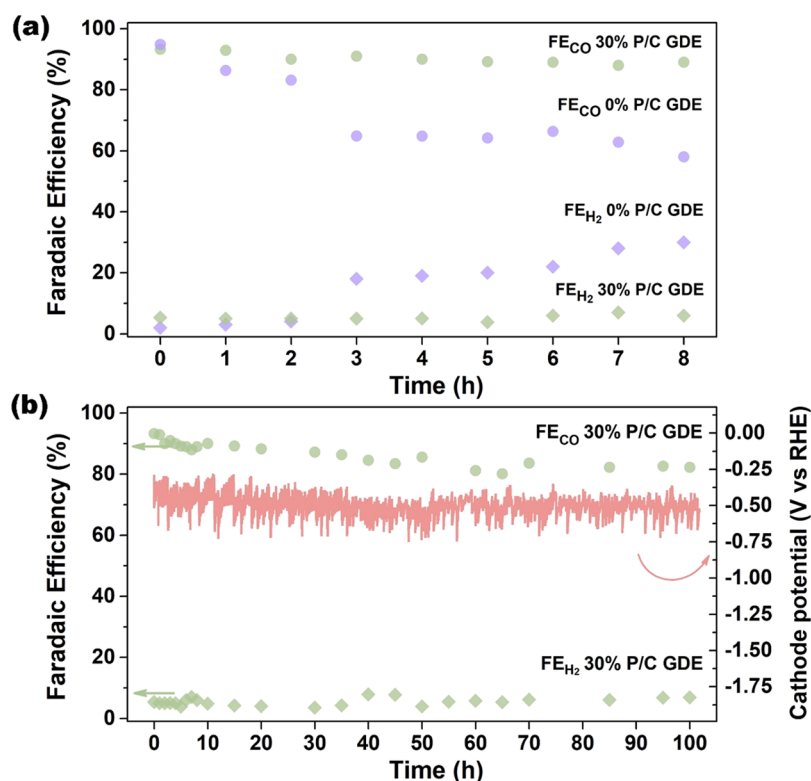
Figure 3. Electrolyzer performance stability tests over 8 and 100 h. (a) Faradaic efficiency for CO and H_2 with the 0% P/C GDE and 30% P/C GDE during an 8 h CO_2 electrolysis experiment at a current density of 100 mA·cm^{-2}. (b) Faradaic efficiency for CO and H_2 and cathode potential for the 30% P/C GDE experiment in an additional 100 h test at a current density of 100 mA·cm^{-2}. The X% P/C represents constant 10 mg carbon black mixed with the X% PTFE weight ratio in the 10 mL suspension for the infiltration, except 0% P/C represents 10 mL of pure water infiltrated through the gas diffusion layers (GDLs).

obtained from mercury intrusion porosimetry (MIP) in Figure 1f show the PSD of the 0% P/C GDL has the most volume in pores of size ranges 10−100 μm and 20−40 nm (MIP cumulative intrusion plot included in Figure S6), which we expect to be in the carbon cloth and MPL, respectively. The MIP data in Table S1 shows the 30% P/C GDL had 11% less total pore volume than the 0% P/C GDL. The PSDs in Figure 1f show the added PTFE and carbon black particles in 30% P/C sample occupied pores in the micrometer range, primarily in the carbon cloth layer. These MIP results provide additional evidence that the 200−400 nm-sized PTFE particles can move relatively freely through the large carbon cloth pores during the vacuum-assisted infiltration but become lodged at the interface to the MPL (as illustrated in Figure 1a and Figure 1c).

To prepare GDE, we deposited the silver catalyst layer on the GDL samples by air-brushed spray coating an ink of silver nanoparticles (Ag NPs), carbon black, and Nafion ionomer onto the MPL surface. Figure S7a−d shows that this method distributed the Ag NPs evenly on a micrometer-scale across the MPLs of 0% P/C and 30% P/C GDEs. We estimated the thickness of the catalyst layers to be approximately 15 μm from the cross-section SEM images (Figure S7f,h) and the Ag elemental maps from SEM-EDS (Figure S7e,g). There is no apparent difference in the top surface of the catalyst layers of the 0% P/C and 30% P/C GDEs.

The CO_2RR to CO performance of the control 0% P/C GDE and the PTFE-embedded 30% P/C GDEs was compared in a sandwich-type flow cell electrolyzer with a single-pass 0.1 M KHCO$_3$ catholyte flow (Figure S8). The cell was completed with an IrO_2 coated titanium plate anode, a 1 M KOH anolyte,

and a Nafion 117 membrane. We measured the catholyte seepage rate through the GDEs using the recently reported method.[34] Briefly, we separated and collected any liquid carried out with gases from the cathode chamber in a two-neck Erlenmeyer flask placed on an analytical balance (Figure S9). An overall schematic of the flow cell electrolyzer and effluent measurements system is provided in Figure S10.

Figure 2 compares the CO_2RR to CO performance of the 0% P/C GDE and the 30% P/C GDE, with the cathode potentials for these tests summarized in Figure S11. At current densities less than 150 mA·cm^{-2}, the CO_2RR product selectivity (Figure 2a) is similar for the 0% P/C and 30% P/C GDEs, with FEs close to 90% for CO and less than 10% for H_2. We did not observe electrolyte seepage from the cathodes at current densities below 150 mA·cm^{-2} (Figure 2b). However, at current densities above 150 mA·cm^{-2}, the 30% P/C GDE was more CO selective than the 0% P/C GDE. For example, at 200 mA·cm^{-2}, the FE$_{CO}$ remained 97.2 ± 1.5% for 30% P/C GDE but dropped to 86.3 ± 2.2% for 0% P/C GDE. At 300 mA·cm^{-2}, the FE$_{CO}$ achieved was 79.5 ± 2.8% for 30% P/C GDE and only 55.0 ± 5.1% for the 0% P/C GDE. We also observed some formate in the liquid products at current densities above 150 mA·cm^{-2}, and its selectivity increased with current densities. Formate production during CO_2RR is common on the Ag-based catalyst.[35]

The main difference in the selectivity of the two GDEs is observed in the H_2 produced at the higher current densities, which is likely due to the electrode flooding that reduces the local CO_2 availability within the catalyst layer.[24] The trend in H_2 production rates is consistent with the seepage rates shown
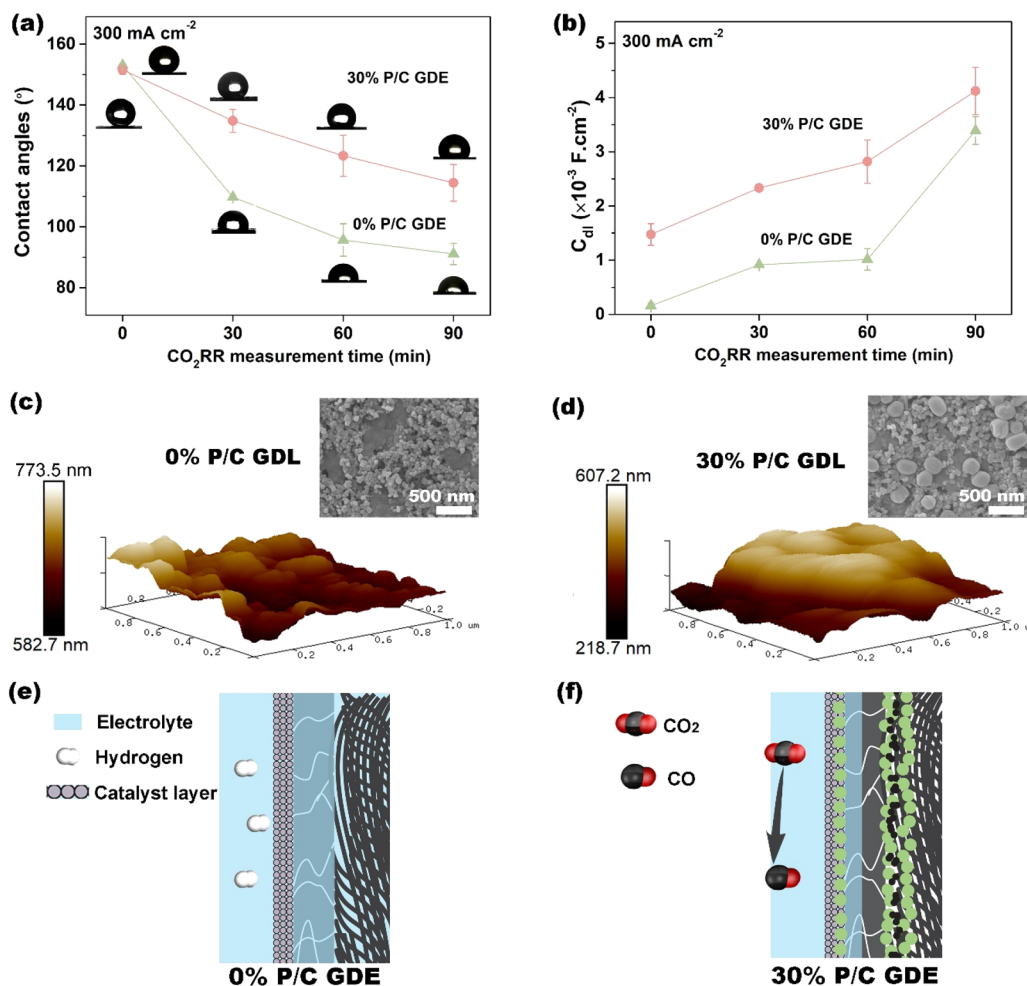
Figure 4. Changes in hydrophobicity and specific double layer capacitance (C_{dl}) of the gas diffusion electrodes (GDEs) after exposure to CO_2 electrolysis conditions. (a) Change in wetting contact angles on the catalyst layer of the 0% P/C and 30% P/C GDEs after CO_2 electrolysis at 300 mA·cm^{-2} for 30, 60, and 90 min. The 0 min sample is a freshly prepared GDE that has not been used in the electrolyzer. The error bars on contact angle data points represent the standard deviation of nine drop measurements on three areas of three independently prepared GDEs. (b) Specific double layer capacitance of 0% P/C and 30% P/C GDEs before and after CO_2 electrolysis at 300 mA·cm^{-2} for 30, 60, and 90 min. C_{dl} calculated from electrochemical surface area as described in the Supporting Information. Error bars in (b) represent the standard deviation of three independent measurements. (c) and (d) Topographic images from atomic force microscope (AFM) scans of $1 \times 1 \mu m^2$ areas of the microporous layer (MPL) of (c) the 0% P/C gas diffusion layer (GDL) and (d) the 30% P/C GDL. (e) and (f) Schematic representations of the interactions of H_2 and CO_2 species with the electrochemically active surface area during CO_2 electrolysis of the gas diffusion electrodes (GDEs) without the hydrophobic particles in (e) 0% P/C GDE and (f) 30% P/C GDE. The X% P/C represents constant 10 mg carbon black mixed with the X% PTFE weight ratio in the 10 mL suspension for the infiltration, except 0% P/C represents 10 mL of pure water infiltrated through the GDLs.

in Figure 2b, with the hydrophobic PTFE-embedded GDE more resistant to electrolyte flooding. For example, at 300 mA·cm^{-2}, the 30% P/C GDE exhibited a seepage rate 9.7 times lower than the seepage rate through 30% P/C GDE, which contributed to the falling catholyte mass transfer resistance from the additional layer.

On the other hand, the CO_2 permeance from the carbon cloth to MPL was measured for 30% P/C and 0% P/C, respectively, as shown in Figure S15. The gas permeance of 30% P/C GDL slightly decreased due to the lower porosity in carbon cloth (Figure 1f), which further led to lower CO selectivity than the 0% P/C GDE at 100 mA·cm^{-2} (Figure 2a). With the flooding promoted at high current densities, however, the tiny advantage was eliminated by the electrode flooding MPL that substantially increased the resistance of CO_2 transfer to the catalyst and promoted H_2 production. Consequently, the 30% P/C GDE electrode can achieve a FE_{CO} nearly 80% at

300 mA cm^{-2}, much higher than the 0% P/C GDE with a FE_{CO} of 55.0 ± 5.1%. Based on the above observations, we postulate that the enhanced CO selectivity results from the hydrophobic PTFE particles embedded at the MPL-GDL interface by the vacuum-assisted infiltration method. These features restrict flooding of the GDE across the MPL layer.

As the largest difference in the FE_{CO} between the 0% P/C and the 30% P/C GDEs was at current densities of 300 mA·cm^{-2}, we used this condition as an operating point to study the effects of PTFE loadings on the performance. Figure 2c shows that increasing the loading of PTFE led to higher FECO and lower rates of HER. Again, this trend likely arises from the role of the PTFE particles at the catalyst-MPL interface that creates a hydrophobic microenvironment in the catalyst layer for efficient gas transport while maintaining a high electrochemical surface area for CO_2RR. As shown in Figure 2d, the seepage rate of GDEs dropped with a higher PTFE content. In other

words, more PTFE in the interface between MPL and carbon cloth makes the GDE more resistant to flooding and thus improves the CO_2RR efficiency.

The orientation of the GDL during the vacuum-assisted infiltration is crucial to depositing the PTFE particles at the optimum location in the GDL. If the GDL is orientated with the microporous layer facing up in the vacuum apparatus (Figure S12), the PTFE particles simply cover the surface of the MPL (Figure S12b). Subsequent deposition of the catalyst layer on this PTFE-coated MPL structure leads to an electrode with poorer electrical conductivity, low CO selectivity (FE_{CO} = 38.1 ± 3.5%), and high HER rates (FE_{H2} = 50.2 ± 5.8%). This additional experiment highlights that the excellent flooding resistance and CO_2RR achieved with the PTFE-embedded GDE are not solely related to the total amount of PTFE added to the electrode but depend on precisely where the PTFE particles deposit.

The electrolyzer stability tests performed at 100 mA cm^{-2} reported in Figure 3a show that the control 0% P/C GDE can sustain a FE_{CO} above 80% for the first 2 h of operation, but after 3 h, the rate of H_2 production increased significantly. In contrast, the 30% P/C GDE maintained a FE_{CO} of 90% for at least 8 h. These results show the enhanced resistance to electrode flooding of the 30% P/C GDE improved the electrode stability remarkably. We repeated the stability test at 100 mA cm^{-2} with 30% P/C GDE for an extended period of 100 h (Figure 3b). We found that the FECO remained above 82.2% even after 100 h with no significant degradation in the cathode cell potential (remained around −0.5 V vs RHE). Figure S13 highlights that the performance of 30% P/C GDE is among the most stable Ag-based electrodes achieving a FE_{CO} above 70% in the liquid flow cell CO_2 electrolyzer at current densities above 100 mA·cm^{-2} reported in the literature.[10,19,31,36−39] We acknowledge that a 100 h operation is well short of the targets of several thousand hours operation required for industrial CO_2 electrolyzers.[40] There are a limited number of reports of CO_2 flow cell electrolyzers for CO production operated for more than 100 h, but the studies that achieved a FE_{CO} greater than 80% were conducted at current densities below 100 mA·cm^{-2}, for example the 4380 h test at 50 mA·cm^{-2} by Kutz et al.[41]

The previous section demonstrated that the PTFE-embedded GDE achieved higher Faradaic efficiencies for much longer durations than the control GDE. Next, we closely examine how the PTFE treatment impacts the hydrophobicity and electrochemically active surface area (ECSA) of GDE. We studied the hydrophobicity using a sessile drop method to measure the water contact angles on the surface of the catalysts layer. As shown in Figure 4a, both the 0% P/C and 30% P/C GDEs were hydrophobic before use in the CO_2 electrolyzer, with water contact angles over 150°. The high hydrophobicity can be attributed to the similar roughness of the catalyst layer (Figures S7 and S16).[42,43] We performed a series of CO_2 electrolysis experiments at 300 mA·cm^{-2} with GDEs exposed to the CO_2RR conditions for 30, 60, and 90 min. After these exposure times, the GDEs were rinsed of excess catholyte off the catalyst layer and then dried. We observed that the contact angles of the catalyst layer for both electrodes decreased with increasing exposure time to CO_2RR conditioning (Figure 4a). The permanent contact angle loss is likely due to degradation of hydrophobic PTFE and carbon black in the catalyst layer when charged by the negative potential.[5,13,44] This observation is consistent with our previous and others results[29,34] and

linked to the increment of electrolyte flooding.[14,45] Nevertheless, the contact angle of the 0% P/C GDE decreased faster and to a lower angle after 90 min (91.4 ± 3.5°) than the 30% P/C GDE, which remained hydrophobic after 90 min of CO_2 electrolysis (contact angle = 114.4 ± 6.0°). The lower contact angles drop over 30% P/C GDE (Figure 4a) could arise from the experience of more positive cathode potentials (−0.85 V vs RHE) than 0% P/C GDE (−1.04 V vs RHE) at 300 mA·cm^{-2} (Figure S11). These experiments confirm that the 30% P/C GDE retains its hydrophobicity for longer than the 0% P/C GDE, but a more detailed study is required to understand better why the PTFE in the carbon cloth layer and protruding into the CL has such a profound impact on the stability of the CL's hydrophobicity.

Many other studies that report an increase in electrode hydrophobicity also report that this hydrophobicity comes with a reduced electrochemically active surface area (ECSA),[24,46] which is generally detrimental to CO_2RR performance.[47] Figure 4b shows the ECSAs that we estimated from the specific double-layer capacitance (C_{dl}) of our 0% P/C and 30% P/C GDEs increase with the duration of CO_2 electrolysis at 300 mA·cm^{-2}. Such enhancement of ECSA is ascribed to the hydrophobicity loss (Figure 4a) due to the degradation of Nafion and carbon black in the catalyst layer as stated before and then leads to an increase in electrolyte-catalyst contact within the catalyst layer. Notably, the ECSAs of the hydrophobic 30% P/C GDE are larger than 0% P/C across the testing conditions, which is highly desired for GDE development.[12] The improvement of the ECSA may be explained by the expansion of the surface area at the MPL. PTFE particles (Figure 1d) that passed through the MPL cracks during the infiltration enhance the roughness of the MPL considerably (see Figure 4c,d, Figure S16a,b). After the catalyst is deposited, the particles covered by the catalyst layer hardly change the surface roughness of the catalyst layer (see Figure S16c,d). The higher roughness comes with an enlarged surface area. More impressively, our results provide another possibility to recognize the relationship: the variation trend of ECSA may not always be consistent with the surface hydrophobicity.

As illustrated in Figure 4e,f, these PTFE particles protruding into the catalyst layer increase the active area for the reaction (ECSA) at a constant Ag loading, which improves the CO selectivity (Figure 2a). Most importantly, the 30% P/C GDE can prevent GDE from serious flooding during CO_2 electrolysis. Maintaining both these properties is important to ensure a high local CO_2 availability and active surface for CO_2RR at industrially applicable current densities.

In conclusion, we used a vacuum-assisted infiltration method to embed PTFE particles in commercial GDLs, and this structure improved the performance of these GDLs as supports for CO_2 electrolysis cathodes. This method embedded the PTFE particles at the interface of the microporous layer and the carbon cloth, and some PTFE particles passed through cracks in the MPL to protrude into the catalyst layer. The protruding PTFE particles led to increased surface areas in the catalyst layer that we subsequently deposited on the GDL. The PTFE-embedded GDEs exhibited excellent selectivity for CO_2 electrolysis to CO at high current densities and outstanding resistance to electrolyte flooding. The PTFE-embedded 30% P/C GDE was able to maintain the FE_{CO} above 80% for more than 100 operating hours at 100 mA·cm^{-2}. This work provides an avenue to tailor commercially available GDLs to the

requirements of CO_2 electrolyzers and paves the way for the large-scale application of carbon-based GDE.

ASSOCIATED CONTENT

ⓈⒾ Supporting Information

The Supporting Information is available free of charge at https://pubs.acs.org/doi/10.1021/acsenergylett.2c01555.

> Experimental materials and methods including schematic and photograph of electrolyzer apparatus; additional SEM images and EDS elemental maps of fluorine; cumulative pore size distribution results from mercury intrusion porosimetry; cathode potential of 0% P/C and 30% P/C gas diffusion electrodes vs current density; comparison of FE_{CO} observed in our 100 h stability test with other Ag-based GDEs reported in literature; calculation method and results for electrochemical active surface area (ECSA); gas permeance results for CO_2 flow in gas diffusion electrodes; surface roughness contours obtained from optical profiler; additional contact angle measurement data; partial current density for CO of 0% P/C and 30% P/C electrolyzer tests; and supporting references (PDF)

AUTHOR INFORMATION

Corresponding Authors

Mengran Li − *Materials for Energy Conversion and Storage (MECS), Department of Chemical Engineering, Faculty of Applied Sciences, Delft University of Technology, 2629 HZ Delft, The Netherlands;* ⓞ orcid.org/0000-0001-7858-0533; Email: m.li-8@tudelft.nl

Thomas E. Rufford − *School of Chemical Engineering, The University of Queensland, St. Lucia 4072, Australia;* ⓞ orcid.org/0000-0002-8865-7976; Email: t.rufford@uq.edu.au

Authors

Yuming Wu − *School of Chemical Engineering, The University of Queensland, St. Lucia 4072, Australia*

Liam Charlesworth − *School of Chemical Engineering, The University of Queensland, St. Lucia 4072, Australia*

Irving Maglaya − *School of Chemical Engineering, The University of Queensland, St. Lucia 4072, Australia*

Mohamed Nazmi Idros − *School of Chemical Engineering, The University of Queensland, St. Lucia 4072, Australia*

Thomas Burdyny − *Materials for Energy Conversion and Storage (MECS), Department of Chemical Engineering, Faculty of Applied Sciences, Delft University of Technology, 2629 HZ Delft, The Netherlands;* ⓞ orcid.org/0000-0001-8057-9558

Geoff Wang − *School of Chemical Engineering, The University of Queensland, St. Lucia 4072, Australia*

Complete contact information is available at:
https://pubs.acs.org/10.1021/acsenergylett.2c01555

Notes

The authors declare no competing financial interest.

ACKNOWLEDGMENTS

REFERENCES

(1) Peter, S. C. Reduction of CO2 to Chemicals and Fuels: A Solution to Global Warming and Energy Crisis. *ACS Energy Letters* **2018**, *3* (7), 1557−1561.

(2) Jouny, M.; Hutchings, G. S.; Jiao, F. Carbon monoxide electroreduction as an emerging platform for carbon utilization. *Nature Catalysis* **2019**, *2* (12), 1062−1070.

(3) Garg, S.; Li, M.; Weber, A. Z.; Ge, L.; Li, L.; Rudolph, V.; Wang, G.; Rufford, T. E. Advances and challenges in electrochemical CO 2 reduction processes: an engineering and design perspective looking beyond new catalyst materials. *Journal of Materials Chemistry A* **2020**, *8* (4), 1511−1544.

(4) Ma, M.; Clark, E. L.; Therkildsen, K. T.; Dalsgaard, S.; Chorkendorff, I.; Seger, B. Insights into the carbon balance for CO2 electroreduction on Cu using gas diffusion electrode reactor designs. *Energy Environ. Sci.* **2020**, *13* (3), 977−985.

(5) Burdyny, T.; Smith, W. A. CO2 reduction on gas-diffusion electrodes and why catalytic performance must be assessed at commercially-relevant conditions. *Energy Environ. Sci.* **2019**, *12* (5), 1442−1453.

(6) Fenwick, A. Q.; Welch, A. J.; Li, X.; Sullivan, I.; DuChene, J. S.; Xiang, C.; Atwater, H. A. Probing the Catalytically Active Region in a Nanoporous Gold Gas Diffusion Electrode for Highly Selective Carbon Dioxide Reduction. *ACS Energy Letters* **2022**, *7* (2), 871−879.

(7) Weng, L.-C.; Bell, A. T.; Weber, A. Z. Modeling gas-diffusion electrodes for CO2 reduction. *Phys. Chem. Chem. Phys.* **2018**, *20* (25), 16973−16984.

(8) Higgins, D.; Hahn, C.; Xiang, C.; Jaramillo, T. F.; Weber, A. Z. Gas-Diffusion Electrodes for Carbon Dioxide Reduction: A New Paradigm. *ACS Energy Letters* **2019**, *4* (1), 317−324.

(9) Zhang, J.; Luo, W.; Züttel, A. Self-supported copper-based gas diffusion electrodes for CO2 electrochemical reduction. *Journal of Materials Chemistry A* **2019**, *7* (46), 26285−26292.

(10) Kim, B.; Hillman, F.; Ariyoshi, M.; Fujikawa, S.; Kenis, P. J. A. Effects of composition of the micro porous layer and the substrate on performance in the electrochemical reduction of CO2 to CO. *J. Power Sources* **2016**, *312*, 192−198.

(11) Nwabara, U. O.; de Heer, M. P.; Cofell, E. R.; Verma, S.; Negro, E.; Kenis, P. J. A. Towards accelerated durability testing protocols for CO2 electrolysis. *Journal of Materials Chemistry A* **2020**, *8* (43), 22557−22571.

(12) Li, M.; Idros, M. N.; Wu, Y.; Burdyny, T.; Garg, S.; Zhao, X. S.; Wang, G.; Rufford, T. E. The role of electrode wettability in electrochemical reduction of carbon dioxide. *Journal of Materials Chemistry A* **2021**, *9* (35), 19369−19409.

(13) Kamat, P.; Christopher, P. Gas Diffusion Electrodes for CO2 and N2 Reduction: A Virtual Issue. *ACS Energy Letters* **2022**, *7* (4), 1469−1472.

(14) Cofell, E. R.; Nwabara, U. O.; Bhargava, S. S.; Henckel, D. E.; Kenis, P. J. A. Investigation of Electrolyte-Dependent Carbonate Formation on Gas Diffusion Electrodes for CO2 Electrolysis. *ACS Appl. Mater. Interfaces* **2021**, *13* (13), 15132−15142.

(15) Nwabara, U. O.; Cofell, E. R.; Verma, S.; Negro, E.; Kenis, P. J. A. Durable Cathodes and Electrolyzers for the Efficient Aqueous Electrochemical Reduction of CO2. *ChemSusChem* **2020**, *13* (5), 855−875.

(16) Yang, K.; Kas, R.; Smith, W. A.; Burdyny, T. Role of the Carbon-Based Gas Diffusion Layer on Flooding in a Gas Diffusion Electrode Cell for Electrochemical CO2 Reduction. *ACS Energy Letters* **2021**, *6* (1), 33−40.

(17) Nguyen, T. N.; Dinh, C.-T. Gas diffusion electrode design for electrochemical carbon dioxide reduction. *Chem. Soc. Rev.* **2020**, *49* (21), 7488−7504.

(18) Vennekoetter, J.-B.; Sengpiel, R.; Wessling, M. Beyond the catalyst: How electrode and reactor design determine the product spectrum during electrochemical CO2 reduction. *Chemical Engineering Journal* **2019**, *364*, 89−101.

(19) Verma, S.; Hamasaki, Y.; Kim, C.; Huang, W.; Lu, S.; Jhong, H.-R. M.; Gewirth, A. A.; Fujigaya, T.; Nakashima, N.; Kenis, P. J. A. Insights into the Low Overpotential Electroreduction of CO2 to CO on a Supported Gold Catalyst in an Alkaline Flow Electrolyzer. *ACS Energy Letters* **2018**, *3* (1), 193−198.

(20) Bejtka, K.; Zeng, J.; Sacco, A.; Castellino, M.; Hernández, S.; Farkhondehfal, M. A.; Savino, U.; Ansaloni, S.; Pirri, C. F.; Chiodoni, A. Chainlike Mesoporous SnO2 as a Well-Performing Catalyst for Electrochemical CO2 Reduction. *ACS Applied Energy Materials* **2019**, *2* (5), 3081−3091.

(21) Chen, X.; Chen, J.; Alghoraibi, N. M.; Henckel, D. A.; Zhang, R.; Nwabara, U. O.; Madsen, K. E.; Kenis, P. J. A.; Zimmerman, S. C.; Gewirth, A. A. Electrochemical CO2-to-ethylene conversion on polyamine-incorporated Cu electrodes. *Nature Catalysis* **2021**, *4* (1), 20−27.

(22) Li, H.; Tang, Y.; Wang, Z.; Shi, Z.; Wu, S.; Song, D.; Zhang, J.; Fatih, K.; Zhang, J.; Wang, H.; Liu, Z.; Abouatallah, R.; Mazza, A. A review of water flooding issues in the proton exchange membrane fuel cell. *J. Power Sources* **2008**, *178* (1), 103−117.

(23) Leonard, M. E.; Orella, M. J.; Aiello, N.; Román-Leshkov, Y.; Forner-Cuenca, A.; Brushett, F. R. Editors' Choice—Flooded by Success: On the Role of Electrode Wettability in CO < sub > 2</sub> Electrolyzers that Generate Liquid Products. *J. Electrochem. Soc.* **2020**, *167* (12), 124521.

(24) Leonard, M. E.; Clarke, L. E.; Forner-Cuenca, A.; Brown, S. M.; Brushett, F. R. Investigating Electrode Flooding in a Flowing Electrolyte, Gas-Fed Carbon Dioxide Electrolyzer. *ChemSusChem* **2020**, *13* (2), 400−411.

(25) Chen, Z.; Pan, W.; Yao, D.; Gao, M.; Gao, Y.; Chen, X.; Krzywanski, J.; Wang, F. Crack evolution during the film drying process of fuel cell microporous layer ink. *Colloids Surf., A* **2022**, *650*, 129283.

(26) Pan, W.; Chen, Z.; Yao, D.; Chen, X.; Wang, F.; Dai, G. Microstructure and macroscopic rheology of microporous layer nanoinks for PEM fuel cells. *Chem. Eng. Sci.* **2021**, *246*, 117001.

(27) Xing, Z.; Hu, L.; Ripatti, D. S.; Hu, X.; Feng, X. Enhancing carbon dioxide gas-diffusion electrolysis by creating a hydrophobic catalyst microenvironment. *Nat. Commun.* **2021**, *12* (1), 136.

(28) Ma, W.; Xie, S.; Liu, T.; Fan, Q.; Ye, J.; Sun, F.; Jiang, Z.; Zhang, Q.; Cheng, J.; Wang, Y. Electrocatalytic reduction of CO2 to ethylene and ethanol through hydrogen-assisted C−C coupling over fluorine-modified copper. *Nature Catalysis* **2020**, *3* (6), 478−487.

(29) Shi, R.; Guo, J.; Zhang, X.; Waterhouse, G. I. N.; Han, Z.; Zhao, Y.; Shang, L.; Zhou, C.; Jiang, L.; Zhang, T. Efficient wettability-controlled electroreduction of CO2 to CO at Au/C interfaces. *Nat. Commun.* **2020**, *11* (1), 3028.

(30) Wakerley, D.; Lamaison, S.; Wicks, J.; Clemens, A.; Feaster, J.; Corral, D.; Jaffer, S. A.; Sarkar, A.; Fontecave, M.; Duoss, E. B.; Baker, S.; Sargent, E. H.; Jaramillo, T. F.; Hahn, C. Gas diffusion electrodes, reactor designs and key metrics of low-temperature CO2 electrolysers. *Nature Energy* **2022**, *7* (2), 130−143.

(31) Dinh, C.-T.; García de Arquer, F. P.; Sinton, D.; Sargent, E. H. High Rate, Selective, and Stable Electroreduction of CO2 to CO in Basic and Neutral Media. *ACS Energy Letters* **2018**, *3* (11), 2835−2840.

(32) García de Arquer, F. P.; Dinh, C.-T.; Ozden, A.; Wicks, J.; McCallum, C.; Kirmani, A. R.; Nam, D.-H.; Gabardo, C.; Seifitokaldani, A.; Wang, X.; Li, Y. C.; Li, F.; Edwards, J.; Richter, L. J.; Thorpe, S. J.; Sinton, D.; Sargent, E. H. CO2 electrolysis to multicarbon products at activities greater than 1 A cm− 2. *Science* **2020**, *367* (6478), 661.

(33) Baumgartner, L. M.; Koopman, C. I.; Forner-Cuenca, A.; Vermaas, D. A. Narrow Pressure Stability Window of Gas Diffusion Electrodes Limits the Scale-Up of CO2 Electrolyzers. *ACS Sustainable Chem. Eng.* **2022**, *10* (14), 4683−4693.

(34) Wu, Y.; Garg, S.; Li, M.; Idros, M. N.; Li, Z.; Lin, R.; Chen, J.; Wang, G.; Rufford, T. E. Effects of microporous layer on electrolyte flooding in gas diffusion electrodes and selectivity of CO2 electrolysis to CO. *J. Power Sources* **2022**, *522*, 230998.

(35) Philips, M. F.; Gruter, G.-J. M.; Koper, M. T. M.; Schouten, K. J. P. Optimizing the Electrochemical Reduction of CO2 to Formate: A State-of-the-Art Analysis. *ACS Sustainable Chem. Eng.* **2020**, *8* (41), 15430−15444.

(36) Jiang, K.; Siahrostami, S.; Zheng, T.; Hu, Y.; Hwang, S.; Stavitski, E.; Peng, Y.; Dynes, J.; Gangisetty, M.; Su, D.; Attenkofer, K.; Wang, H. Isolated Ni single atoms in graphene nanosheets for high-performance CO2 reduction. *Energy Environ. Sci.* **2018**, *11* (4), 893−903.

(37) Zheng, T.; Jiang, K.; Ta, N.; Hu, Y.; Zeng, J.; Liu, J.; Wang, H. Large-Scale and Highly Selective CO2 Electrocatalytic Reduction on Nickel Single-Atom Catalyst. *Joule* **2019**, *3* (1), 265−278.

(38) Lu, X.; Jiang, Z.; Yuan, X.; Wu, Y.; Malpass-Evans, R.; Zhong, Y.; Liang, Y.; McKeown, N. B.; Wang, H. A bio-inspired O2-tolerant catalytic CO2 reduction electrode. *Science Bulletin* **2019**, *64* (24), 1890−1895.

(39) Asadi, M.; Kim, K.; Liu, C.; Addepalli Aditya, V.; Abbasi, P.; Yasaei, P.; Phillips, P.; Behranginia, A.; Cerrato José, M.; Haasch, R.; Zapol, P.; Kumar, B.; Klie Robert, F.; Abiade, J.; Curtiss Larry, A.; Salehi-Khojin, A. Nanostructured transition metal dichalcogenide electrocatalysts for CO2 reduction in ionic liquid. *Science* **2016**, *353* (6298), 467−470.

(40) Masel, R. I.; Liu, Z.; Yang, H.; Kaczur, J. J.; Carrillo, D.; Ren, S.; Salvatore, D.; Berlinguette, C. P. An industrial perspective on catalysts for low-temperature CO2 electrolysis. *Nat. Nanotechnol.* **2021**, *16* (2), 118−128.

(41) Kutz, R. B.; Chen, Q.; Yang, H.; Sajjad, S. D.; Liu, Z.; Masel, I. R. Sustainion Imidazolium-Functionalized Polymers for Carbon Dioxide Electrolysis. *Energy Technology* **2017**, *5* (6), 929−936.

(42) Jaiswal, J.; Singh; Ramesh Chandra, M.; Sanger, A.; Kumar, A.; Mourya, S.; Chauhan, S.; Daipuriya, R. Enhanced Optical Absorbance Of Hydrophobic Ti Thin Film: Role Of Surface Roughness. *Advanced Materials Letters* **2016**, *7* (6), 485−490.

(43) Gong, X.; Zhang, L.; He, S.; Jiang, S.; Wang, W.; Wu, Y. Rewritable superhydrophobic coatings fabricated using water-soluble polyvinyl alcohol. *Materials & Design* **2020**, *196*, 109112.

(44) Yang, H.; Hu, Y.-w.; Chen, J.-j.; Balogun, M. S.; Fang, P.-p.; Zhang, S.; Chen, J.; Tong, Y. Intermediates Adsorption Engineering of CO2 Electroreduction Reaction in Highly Selective Heterostructure Cu-Based Electrocatalysts for CO Production. *Adv. Energy Mater.* **2019**, *9* (27), 1901396.

(45) Niu, Z.-Z.; Gao, F.-Y.; Zhang, X.-L.; Yang, P.-P.; Liu, R.; Chi, L.-P.; Wu, Z.-Z.; Qin, S.; Yu, X.; Gao, M.-R. Hierarchical Copper with Inherent Hydrophobicity Mitigates Electrode Flooding for High-Rate CO2 Electroreduction to Multicarbon Products. *J. Am. Chem. Soc.* **2021**, *143* (21), 8011−8021.

(46) Li, M.; Idros, M. N.; Wu, Y.; Garg, S.; Gao, S.; Lin, R.; Rabiee, H.; Li, Z.; Ge, L.; Rufford, T. E.; Zhu, Z.; Li, L.; Wang, G. Unveiling the effects of dimensionality of tin oxide-derived catalysts on CO2 reduction by using gas-diffusion electrodes. *Reaction Chemistry & Engineering* **2021**, *6* (2), 345−352.

(47) Mowbray, B. A. W.; Dvorak, D. J.; Taherimakhsousi, N.; Berlinguette, C. P. How Catalyst Dispersion Solvents Affect CO2

Electrolyzer Gas Diffusion Electrodes. *Energy Fuels* **2021**, 35 (23), 19178−19184.

📖 Recommended by ACS

Intermittent Operation of CO_2 Electrolyzers at Industrially Relevant Current Densities

Angelika A. Samu, Csaba Janáky, *et al.*
MAY 04, 2022
ACS ENERGY LETTERS   READ 🗗

Evaluating the Effects of Membranes, Cell Designs, and Flow Configurations on the Performance of Cu-GDEs in Converting CO_2 to CO

Liniker de Sousa, Guido Mul, *et al.*
SEPTEMBER 13, 2022
ACS ES&T ENGINEERING   READ 🗗

Electrochemical Reduction of CO_2 in Tubular Flow Cells under Gas–Liquid Taylor Flow

Isabell Bagemihl, Volkert van Steijn, *et al.*
SEPTEMBER 15, 2022
ACS SUSTAINABLE CHEMISTRY & ENGINEERING   READ 🗗

Electrocatalytic Membranes for Tunable Syngas Production and High-Efficiency Delivery to Biocompatible Electrolytes

Xiaobo Zhu, Zhiyong Jason Ren, *et al.*
APRIL 21, 2021
ACS SUSTAINABLE CHEMISTRY & ENGINEERING   READ 🗗

Get More Suggestions >